*Mineralogical Magazine* (2022), **86**, 447–458
doi:10.1180/mgm.2022.31

CAMBRIDGE UNIVERSITY PRESS

**Article**

# As-bearing new mineral species from Valletta mine, Maira Valley, Piedmont, Italy: IV. Lombardoite, $Ba_2Mn^{3+}(AsO_4)_2(OH)$ and aldomarinoite, $Sr_2Mn^{3+}(AsO_4)_2(OH)$, description and crystal structure

Fernando Cámara[1,2*], Lisa Baratelli[1], Marco E. Ciriotti[3,4], Fabrizio Nestola[5], Gian Carlo Piccoli[6], Ferdinando Bosi[7,8], Erica Bittarello[4,9], Ulf Hålenius[10] and Corrado Balestra[11]

[1]Dipartimento di Scienze della Terra, Università degli Studi di Milano, via Sandro Botticelli 23, 20133 Milano, Italy; [2]CrisDi, Interdepartmental Centre for the Research and Development of Crystallography, via Pietro Giuria 5, I-10125, Torino, Italy; [3]Associazione Micromineralogica Italiana, via San Pietro 55, I-10073 Devesi-Cirié, Torino, Italy; [4]Dipartimento di Scienze della Terra, Università degli Studi di Torino, via Tommaso Valperga Caluso, 10125 Torino, Italy; [5]Dipartimento di Geoscienze, Università degli Studi di Padova, via Giovanni Gradenigo 6, 35131 Padova, Italy; [6]Associazione Micromineralogica Italiana, via Vincenzo Gioberti 16, 12051 Alba, Cuneo, Italy; [7]Dipartimento di Scienze della Terra, Università di Roma, piazzale Aldo Moro 5, I-00185 Roma, Italy; [8]CNR, Istituto di Geologia Ambientale e Geoingegneria, U.O.S. di Roma, Roma, Italy; [9]SpectraLab s.r.l., Academic spin-off of the University of Turin, via Valperga Caluso 35, I-1012519 Torino, Italy; [10]Department of Geosciences, Swedish Museum of Natural History, SE-10805 Stockholm, Sweden; and [11]Associazione Micromineralogica Italiana, via Luigi Delfino 74, I-17017 Millesimo, Savona, Italy

## Abstract

Lombardoite, ideally $Ba_2Mn^{3+}(AsO_4)_2(OH)$, and aldomarinoite, ideally $Sr_2Mn^{3+}(AsO_4)_2(OH)$, are two new minerals of the arsenbrackebuschite group in the brackebuschite supergroup, discovered in Fe–Mn ore in metaquartzites of the abandoned mine of Valletta, Canosio, Val Maira, Cuneo Province, Piedmont, Italy. They occur as red–brown and orange brown, respectively, as subhedral crystals (< 0.5 mm) in thin masses, associated with quartz, aegirine, baryte, calcite, hematite, muscovite and Mn minerals such as cryptomelane, braunite and manganberzeliite. Both minerals are translucent, have yellow–orange streak and vitreous lustre. Both are brittle. Estimated Mohs hardness is 6–6½ for lombardoite (by analogy to canosioite), and 4½–5 for aldomarinoite (by analogy to tokyoite). Calculated densities are 5.124 g/cm$^3$ for lombardoite and 4.679 g/cm$^3$ for aldomarinoite. Both minerals are biaxial (+). Lombardoite shows $2V_z$(meas.) = 78(4)° and is pleochroic with $X$ = yellowish brown, $Y$ = brown and $Z$ = reddish brown ($Z > Y > X$). Aldomarinoite has $2V_z$(meas.) = 67.1(1)°, and is pleochroic with $X$ = brown, $Y$ = brownish orange and $Z$ = yellowish brown ($Z > Y > X$). Point analyses by electron microprobe using wavelength dispersive spectroscopy resulted in the empirical formula (based on 9 O anions): $(Ba_{1.96}Sr_{0.17}Pb_{0.04}Na_{0.02}Ca_{0.02})_{\Sigma 2.21}(Mn^{3+}_{0.62}Fe^{3+}_{0.13}Al_{0.06}Mg_{0.11})_{\Sigma 0.92}[(As_{0.87}V_{0.12}P_{0.01})_{\Sigma 1.00}O_4]_2(OH)$ for lombardoite, and $(Sr_{1.93}Ca_{0.21}Ba_{0.04}Pb_{0.01})_{\Sigma 2.19}(Mn^{3+}_{0.48}Al_{0.35}Fe^{3+}_{0.21}Mg_{0.01})_{\Sigma 1.05}[(As_{0.92}V_{0.03})_{\Sigma 0.95}O_4]_2(OH)$ for aldomarinoite. The absence of $H_2O$ was confirmed by Raman spectroscopy and infrared spectroscopy. Both minerals are monoclinic, $P2_1/m$, with unit-cell parameters $a$ = 7.8636(1) Å, $b$ = 6.13418(1) Å, $c$ = 9.1197(1) Å, β = 112.660(2)° and $V$ = 405.94(1) Å$^3$, for lombardoite and $a$ = 7.5577(4) Å, $b$ = 5.9978(3) Å, $c$ = 8.7387(4) Å, β = 111.938(6)° and $V$ = 367.43(3) Å$^3$, for aldomarinoite. The eight strongest powder X-ray diffraction lines are [$d$, Å ($I_{rel}$) ($hkl$)]: 6.985 (39) (10$\bar{1}$), 3.727 (33) (111), 3.314 (100) (21$\bar{1}$), 3.073 (24) (020), 3.036 (33) (21$\bar{2}$, 10$\bar{3}$), 2.810 (87) (12$\bar{1}$, 112), 2.125 (20) (301, 11$\bar{4}$) and 1.748 (24) (321) for lombardoite and 3.191 (89) (21$\bar{1}$), 2.997 (45) (020), 2.914 (47) (21$\bar{2}$, 10$\bar{3}$), 2.715 (100) (112), 2.087 (39) (12$\bar{3}$, 1.833 (32) (31$\bar{4}$), 1.689 (36) (321), 1.664 (21) (132) for aldomarinoite. The minerals are isostructural with brackebuschite: infinite chains of edge sharing octahedra running parallel to the **b** axis and decorated with $AsO_4$ groups are connected along the **a** and **c** axes through Ba and Sr atoms in lombardoite and aldomarinoite, respectively. The minerals are named after Bruno Lombardo (1944–2014), geologist and petrologist at C.N.R. (National Research Council of Italy), and Aldo Marino (b. 1942) the mineral collector and founding member of the AMI – Italian Micromineralogical Association.

**Keywords:** lombardoite, aldomarinoite, new mineral, manganese arsenate, crystal structure, Raman spectroscopy, infrared spectroscopy, brackebuschite supergroup, Valletta mine, Cuneo, Piedmont, Italy

(Received 13 January 2022; accepted 18 March 2022; Accepted Manuscript published online: 7 April 2022; Associate Editor: Oleg I Siidra)

## Introduction

The discovery of new arsenate mineral species at the Valletta mine dumps, Piedmont, Italy, makes this a significant mineralogical locality. Lombardoite (IMA2016-058, Cámara *et al.*, 2016) and aldomarinoite (IMA2021-054, Cámara *et al.*, 2021) belong to the brackebuschite supergroup of minerals and are the fourth

*Author for correspondence: Fernando Cámara, Email: fernando.camara@unimi.it
**Cite this article:** Cámara F., Baratelli L., Ciriotti M.E., Nestola F., Piccoli G.C., Bosi F., Bittarello E., Hålenius U. and Balestra C. (2022) As-bearing new mineral species from Valletta mine, Maira Valley, Piedmont, Italy: IV. Lombardoite, $Ba_2Mn^{3+}(AsO_4)_2(OH)$ and aldomarinoite, $Sr_2Mn^{3+}(AsO_4)_2(OH)$, description and crystal structure. *Mineralogical Magazine* **86**, 447–458. https://doi.org/10.1180/mgm.2022.31

and the eighth, respectively, of a series of new As-bearing minerals from Valletta Mine (grandaite, $Sr_2Al(AsO_4)_2(OH)$, Cámara *et al.* 2014; braccoite, $NaMn_5^{2+}[Si_5AsO_{17}(OH)](OH)$, Cámara *et al.* 2015; lombardoite, $Ba_2Mn^{3+}(AsO_4)_2(OH)$, Cámara *et al.* 2016; canosioite, $Ba_2Fe^{3+}(AsO_4)_2(OH)$, Cámara *et al.* 2017, aldomarinoite $Sr_2Mn^{3+}(AsO_4)_2(OH)$, Cámara *et al.* 2021; castellaroite, $Mn_3^{2+}(AsO_4)_2{\cdot}4.5H_2O$, Kampf *et al.*, 2016; and rüdlingerite, $Mn_2^{2+}V^{5+}As^{5+}O_7{\cdot}2H_2O$, Roth *et al.* 2020). Aldomarinoite represents the fifth Sr-dominant arsenate of the mineral species approved by the Commission on New Minerals, Nomenclature and Classification of the International Mineralogical Association (IMA-CNMNC), after arsenogoyazite, $SrAl_3(AsO_4)(AsO_3OH)(OH)_6$ (Walenta and Dunn, 1984), grandaite, $Sr_2Al(AsO_4)_2(OH)$ (Cámara *et al.*, 2014), kemmlitzite, $SrAl_3(AsO_4)(SO_4)(OH)_6$ (Hak *et al.*, 1969), oberwolfachite, $SrFe_3^{3+}(AsO_4)(SO_4)(OH)_6$ (Chukanov *et al.*, 2021), strontiopharmacosiderite, $Sr_{0.5}Fe_4^{3+}(AsO_4)_3(OH)_4{\cdot}4H_2O$ (Mills *et al.*, 2014), and the second one, after lombardoite, having dominant $Mn^{3+}$ instead of Al or $Fe^{3+}$ in the arsenbrackebuschite group.

Samples containing lombardoite were collected by Corrado Balestra and Roberto Bracco, whereas aldomarinoite samples were collected by Gian Carlo Piccoli, on the dumps of a dismissed old mine found close to the Valletta pass at the Valletta Valley ('Vallone della Valletta' in Italian) in the Maira Valley, Piedmont, Italy, a small Fe–Mn deposit that has never been studied in detail from a geological or petrological point of view. The name of lombardoite honours Dr. Bruno Lombardo (1944–2014), geologist and petrologist at C.N.R. (National Research Council of Italy), for his extensive and sound contributions on the evolution of orogenic belts worldwide. A fragment of the holotype material is deposited in the mineralogical collections of the Museo Regionale di Scienze Naturali di Torino, Sezione di Mineralogia, Petrografia e Geologia, via Giovanni Giolitti 36, I-10123 Torino, Italy, catalogue number M/U 17111. The name aldomarinoite honours Mr. Aldo Marino, the collector and the founding member of the AMI – Italian Micromineralogical Association, born in Dronero (Cuneo Province) in 1942 who, with Gian Carlo Piccoli, first found the Valletta locality. The holotype material is deposited in the mineral collections of the Museo delle Collezioni di Mineralogia, Gemmologia, Petrologia e Giacimentologia, Dipartimento di Scienze della Terra "Ardito Desio", Università di Milano, Italy, under the catalogue number MCMGPG-H2021–001.

## Geological settings and mineral occurrence

The discovery area of the two minerals is the Valletta mine, 'Vallone della Valletta', Canosio, Val Maira, Cuneo province, Piedmont, Italy (44°23'43"N, 7°5'30"E, 2560 m a.s.l.). The area is geologically located in the Briançonnais Zone of the southern Cottian Alps, not far from the French border line. Geological data of the area are limited and a detailed study of the old mine is missing. The information given here is taken mainly from Crema *et al.* (1971) and Collo (1997). The sequence cropping out at the Valletta mine belongs to the internal units of the Briançonnais Zone (also known as Axial Permian–Carboniferous Zone), and consists of sedimentary detrital deposits and intermediate–acid volcanic activity rocks (Carboniferous–Permian). A quartzitic formation is located above these, comprising quartz conglomerates (Verrucano formation) and arenaceous quartzites. Then the evaporitic sequence (Lower Triassic) and the carbonate platform rocks such as schistose limestones, limestones and dolomites follow. Sedimentation of dolomitic breccias occurs during Upper Triassic followed again by evaporites. Then another transgressive phase occurs, characterised by carbonaceous sedimentation (Cretaceous–Lower Eocene). Finally, the Eocene–Oligocene period consists of calcarenites from detrital and turbidite facies.

In the Valletta mine, the volume of the mineralised body is limited to the surface and the mine dumps are the main remains of the former mining activities (Fig. 1). They consist of yellowish limestones–dolostones and red–brown quartzites and silicoclastic rocks, which contain calcareous, quartzitic and volcanic clasts with variable dimensions from a few millimetres to ~15 centimetres. The quartzitic rocks are composed of quartz conglomerates of the Alpine Verrucano and arenaceous quartzites (Upper Permian–Lower Triassic); the quartzites cover the conglomerates and the fine-grained quartz–feldspar schists derived from the acid volcanism. Above the quartzites, the limestones–dolostones consist of schistose limestones, yellow dolostones and an alternation of limestones and dolostones. From a tectonic point of view, the Valletta area is part of the Marinet anticlinal, or the siliceous Bande de Marinet, the southern tectonic zone of the internal units, and the Sautron unit.

In the mine dumps, the quartzites and the calcareous rocks are often fractured, and show quartz and calcite veins containing mineral phases rich in As, V, Mn, Ba and Sr, which are also present along the fault planes (Fig. 2). These minerals are probably the result of crystallisation from hydrothermal fluids and oxidising conditions, as suggested by the presence of hematite, braunite and cryptomelane.

The present new minerals are associated strictly with quartz, aegirine, baryte, calcite, hematite, muscovite and Mn minerals such as cryptomelane, braunite and manganberzeliite. Other minerals that have been observed in the same locality are: adelite, albite, arseniopleite, azurite, bariopharmacosiderite, berzeliite, bosiite, braccoite, canosioite, caryinite, castellaroite, coralloite, diopside, fianelite, fluorapatite, gamagarite, ganophyllite, grandaite, gypsum, hollandite, ilmenite, magnesio-arfvedsonite, magnesio-riebeckite, magnetite, malachite, mimetite, neotocite, opal, orthoclase, oxy-dravite, palenzonaite, phlogopite, piccoliite, pyrobelonite, ranciéite, rhodochrosite, rhodonite, richterite, rüdlingerite, rutile, saneroite, talc, tetrahedrite series minerals, thorianite, tilasite, tinnunculite, tiragalloite, titanite, tokyoite and wallkilldellite.

## Appearance and physical properties

Lombardoite (Fig. 3) and aldomarinoite (Fig. 4) occur as subhedral crystals in thin masses, a few cm in size, with uneven fracture, or aggregates of small crystals (<0.5 mm), in white veins of compact quartz or along the fault planes, as a reddish-brown quartzitic masses. Well-formed crystals, typically platy tablets, are very rare. Single crystals of lombardoite are dark red–brown, whereas aldomarinoite crystals are dark orange. Both are translucent, have a yellow–orange streak and a vitreous lustre. Lombardoite and aldomarinoite are optically biaxial (+). Lombardoite has $2V_z$(meas.) = 78(4)° and is pleochroic with $X$ = yellowish brown, $Y$ = brown and $Z$ = reddish brown ($Z > Y > X$); the mean refractive index ($n_{ave}$) obtained from the Gladstone–Dale relationship (Mandarino, 1979, 1981) using the empirical formulae and calculated densities is 1.86, which is far beyond our available experimental range. Aldomarinoite has $2V_z$(meas.) = 67.1(1)°, measured using a spindle stage mounted in a Leitz Dialux

**Fig. 1.** Image of mine dumps, the main remains of the former mining activities. Rocca la Meja stands in the background.

**Fig. 3.** Picture of lombardoite: reddish-brown veinlet exposed on quartz (Field of view: 5 mm across, collection and photo R. Bracco).

**Fig. 2.** Typical samples of millimetric orange aggregates, associated with quartz, along a fault plane. They are probably As–Mn minerals characteristic in Valletta Mine.

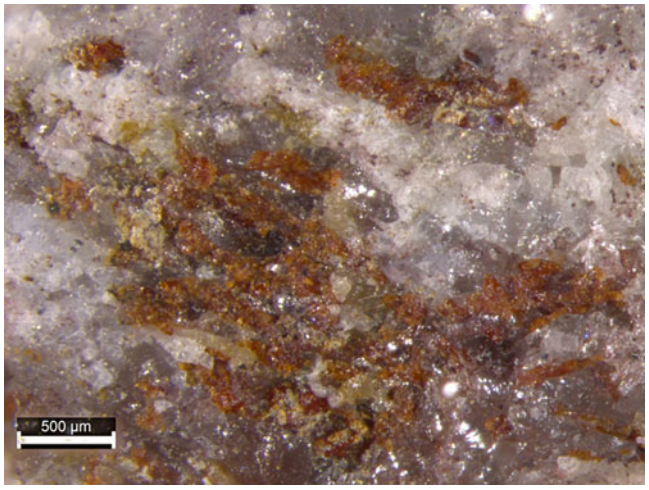


**Fig. 4.** Picture of subhedral crystals of dark orange aldomarinoite and yellow tilasite within a quartz vein from the holotype, catalogue no. MCMGPG-H2021–001 (photo L. Baratelli).

microscope with polarised light, and with optical calculations made with the *Excelibr* spreadsheet (Steven and Gunter, 2018). Aldomarinoite is pleochroic with $X$ = brown, $Y$ = brownish orange and $Z$ = yellowish brown ($Z > Y > X$) and the calculated mean refractive index is 1.83 (from the Gladstone–Dale relationship). Both minerals are brittle, and no cleavage or parting is observed. Hardness was not measured but assigned by analogy to canosioite (6–6½) for lombardoite, and to tokyoite (4½–5) for aldomarinoite. Density was not measured due to the small crystal size and the frequent micro inclusions of other phases. The calculated density obtained from the empirical formula and unit-cell parameters measured during the single-crystal study is 5.124 g/cm$^3$ for lombardoite and 4.679 g/cm$^3$ for aldomarinoite.

## Micro-Raman spectroscopy

The Raman spectrum of lombardoite (Fig. 5, upper spectrum) was obtained using a micro/macro Jobin Yvon Mod. LabRam HRVIS at the University of Torino, whereas the aldomarinoite spectrum (Fig. 5, lower spectrum) was obtained using a high resolution confocal micro-Raman system (LabRam HR Evolution – Horiba at the University of Milano), both equipped with a motorised $x$–$y$ stage. The back-scattered Raman signal was collected with a 50× objective and the Raman spectrum was obtained for a non-oriented crystal. The 532 nm line was used as excitation; laser power was controlled by means of a series of density filters. The system was calibrated using the 520.6 cm$^{-1}$ Raman band of silicon. The spectra were collected with multiple acquisitions (5 to 10 for lombardoite, 3 for aldomarinoite) with single counting times ranging between 10 and 20 s for lombardoite and between 30 and 40 s for aldomarinoite. The spectrum was recorded using the Horiba *LabSpec 5* (lombardoite) and *LabSpec 6* (aldomarinoite) software packages from 100 to 4000 cm$^{-1}$ for lombardoite and from 50 to 4000 cm$^{-1}$ for aldomarinoite, the results of the spectroscopic analysis are reported below.

The presence of $(AsO_4)^{3-}$ is confirmed. Although in many cases it is very difficult to separate the contributions of arsenate from those of vanadate units, a comparative analysis of Raman spectra of other members of the brackebuschite supergroup allows

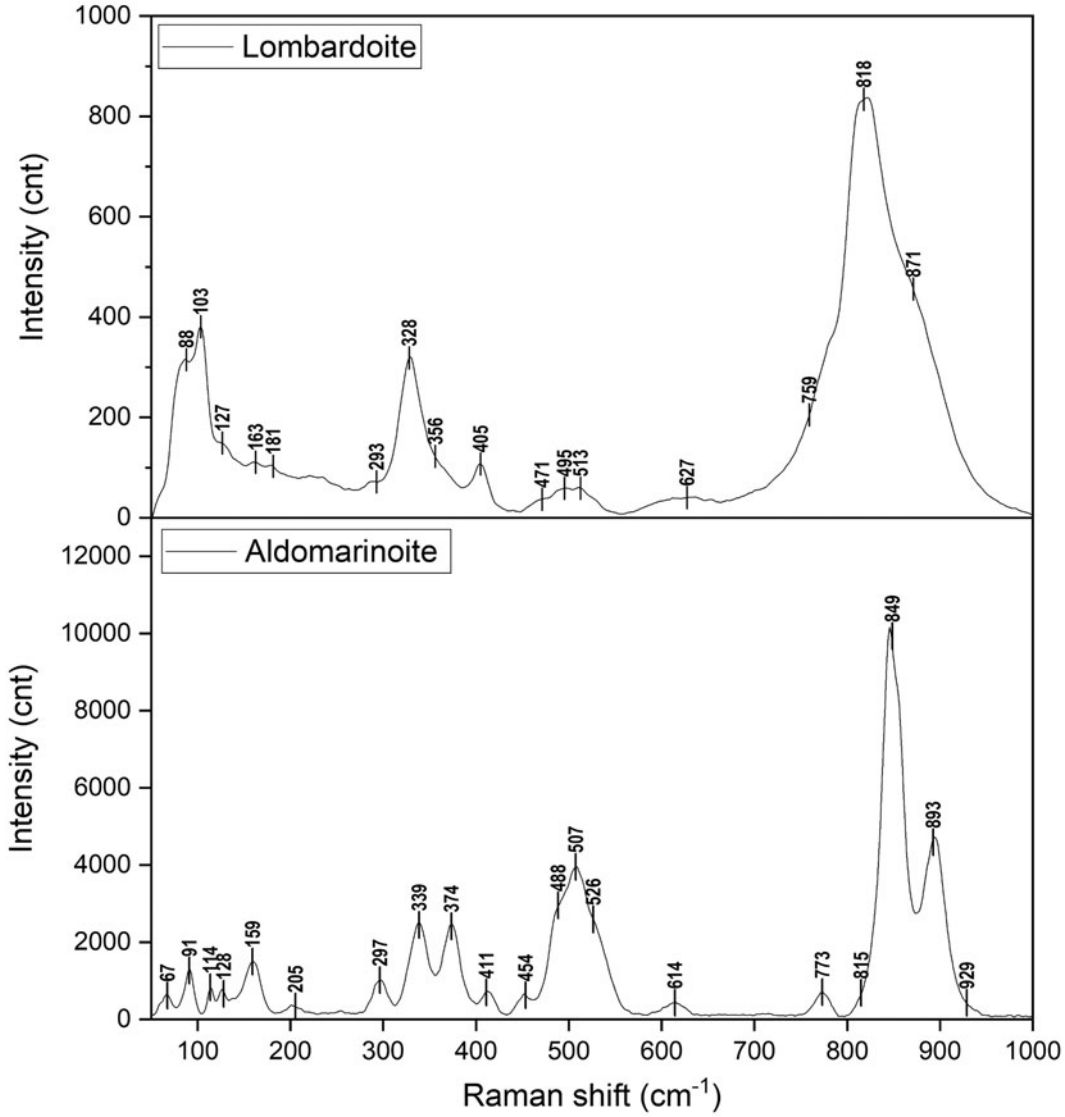


**Fig. 5.** Raman spectra of lombardoite and aldomarinoite in the 50–1000 $cm^{-1}$ region.

the identification of two main bands in the region of 750–950 $cm^{-1}$, centred at ca. 818 and 871 $cm^{-1}$ (plus two weak shoulders at 759 and 914 $cm^{-1}$) for lombardoite and at ca. 848 and 892 $cm^{-1}$ (plus three weak shoulders at 776, 816 and 932 $cm^{-1}$) for aldomarinoite, they are slightly shifted compared to those found for canosioite (838, 862 and 896 $cm^{-1}$, Cámara *et al.*, 2017) and grandaite (at 833, 857 and 899 $cm^{-1}$, Cámara *et al.*, 2014), although the band at ~850 $cm^{-1}$ is not clearly resolved in the Raman spectrum of lombardoite. These two main bands that are convoluted in lombardoite can be assigned to the stretching modes of $(AsO_4)^{3-}$ and $(VO_4)^{3-}$ groups respectively (the 871 $cm^{-1}$ one is weaker due to the lower content of $VO_4$ in lombardoite). A broad and weak band is observed at 627 $cm^{-1}$. Similar band frequencies have been observed for canosioite (Cámara *et al.*, 2017) where multiple bands are shifted to higher frequencies.

In the region 200–600 $cm^{-1}$ multiple Raman bands are observed at 293, 328 and 356 $cm^{-1}$ for lombardoite and at 202, 297, 338 and 374 $cm^{-1}$ for aldomarinoite ($As^{5+}$–O bending vibrations); further bands are observed at 405, 471 and 505 $cm^{-1}$ for lombardoite and at 411, 453, 488, 508, 529 and 612 $cm^{-1}$ for aldomarinoite. Bands lower than 200 $cm^{-1}$ correspond to M–O and lattice modes (88, 103, 163 and 181 $cm^{-1}$ for lombardoite and 67, 91, 114, 126 and 160 $cm^{-1}$ for aldomarinoite).

No bands were observed in the range between 2500 and 4000 $cm^{-1}$ in the Raman spectrum of lombardoite. The absence of strong bands with frequencies higher than 1000 $cm^{-1}$ would indicate the absence of OH groups in lombardoite. Same difficulties on observing bands in the range between 2500 and 4000 $cm^{-1}$ of the Raman spectrum was found in grandaite (Cámara *et al.*, 2014) and canosioite (Cámara *et al.*, 2017). However, a broad band centred at ca. 2970 $cm^{-1}$ was observed in this range in the Raman spectrum of aldomarinoite, which agrees well with the value calculated with the equation $3592-304\times10^{9}\cdot\exp(-d(O\cdots O)/0.1321)$ (Libowitzky, 1999), i.e. 3108 $cm^{-1}$.

## Infrared spectroscopy

Fourier-transformed infrared (FTIR, Fig. 6) transmission spectra (64 scans) of lombardoite were recorded using a diamond anvil cell (High Pressure Diamond Optics, Inc.). They were obtained

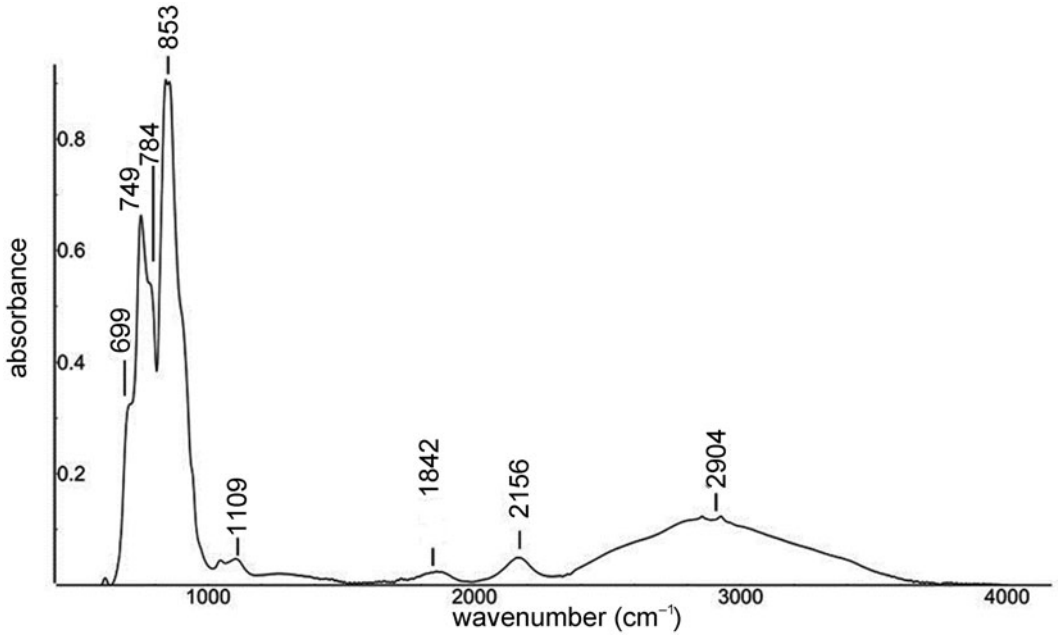


**Fig. 6.** FTIR spectrum of lombardoite in the 600–4000 $cm^{-1}$ region.

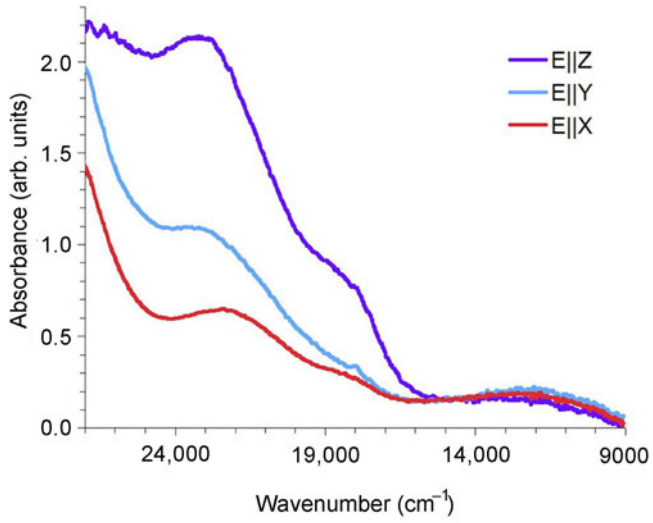


**Fig. 7.** Polarised single-crystal absorption spectra of lombardoite.

with a spectrophotometer Bruker Vertex 70 coupled with a Hyperion 3000 microscope at Centro Conservazione e Restauro "La Venaria Reale" (CCR, Torino, Italy). The instrument is equipped with an MCT detector (Infrared Associates Inc.), working in the spectral range from 4000 to 600 $cm^{-1}$ with an average spectral resolution of 4 $cm^{-1}$. The FTIR spectrum obtained for lombardoite shows the presence of a broad weak band at ~2900 $cm^{-1}$ that could be assigned to the stretching of OH groups. This band agrees well with Raman spectroscopy observations. Thus, in the absence of F in the electron microprobe analysis and on the basis of crystal structure refinement (SREF) data (see below) we also consider the occurrence of (OH) groups in lombardoite. As the FTIR spectrum has no absorption band at ca. 1650 $cm^{-1}$ (e.g. bending vibration) the presence of $H_2O$ groups can be ruled out.

## Optical absorption spectroscopy (OAS)

Polarised optical absorption spectra of double sided polished single-crystal absorbers of lombardoite prepared from X–Y (32 μm thick) and Y–Z (24 μm thick) sections were recorded in the range 9000–34000 $cm^{-1}$ using an AVASPEC-ULS2048X16 spectrometer attached via a 400 μm UV optic fibre cable to a Zeiss Axiotron UV-microscope. A 75 W Xenon arc lamp was used as a light source and Zeiss Ultrafluar 10× lenses served as objective and condenser. The size of the circular measure aperture was 32 μm in diameter. A UV-quality Glan-Thompson prism with a working range from 250 to 2700 nm (40,000 to 3704 $cm^{-1}$) was used as the polariser. The recorded spectra (Fig. 7) show three intense and broad absorption bands at 22,900, 22,100 and 18,300 $cm^{-1}$. An additional broad band of medium intensity occurs at 12,000 $cm^{-1}$. Observed bands and their intensities, band-widths and energies are typical for spin-allowed electronic *d-d* transitions observed in spectra of minerals containing strongly elongated or compressed octahedra occupied by $Mn^{3+}$, for example as observed in piemontite and kanonaite (e.g. Smith *et al.*, 1982). From the observed band energies, the crystal field splitting parameter (10 *Dq*) for $Mn^{3+}$ at the *M*-site of lombardoite is calculated to be 15,100 $cm^{-1}$. This compares very well with 10 *Dq* values in the range 14,400 to 15,600 $cm^{-1}$ for $Mn^{3+}$ in epidote and andalusite-group minerals, suggesting a mean Mn–O bond distance in lombardoite of ~2.02 Å.

## Chemical data

The chemical composition of lombardoite was determined using a Cameca SX-50 electron microprobe in wavelength dispersive spectroscopy (WDS) mode at the Institute of Environmental Geology and Geoengineering (IGAG – C.N.R., Rome) on the same crystal used for structure determination. Major and minor elements were determined at 15 kV accelerating voltage and 15 nA beam current (beam size = 1 μm), with 40 to 20 s counting time on both peak and background. Fluorine, Si, K, Ti, Cr, Ni,

**Table 1.** Analytical data (wt.%) for lombardoite (5 data points) and aldomarinoite (4 data points).

| | Lombardoite | | | | Aldomarinoite | | | |
|---|---|---|---|---|---|---|---|---|
| | Mean | Range | S.D. | Probe standard | Mean | Range | S.D. | Probe standard |
| $As_2O_5$ | 31.48 | 30.95–32.15 | 0.46 | GaAs (*Lα*) | 40.33 | 39.94–40.61 | 0.28 | nickeline (*Lα*) |
| $V_2O_5$ | 3.33 | 3.24–3.44 | 0.10 | vanadinite (*Kα*) | 1.03 | 0.99–1.13 | 0.06 | V metal (*Kα*) |
| $P_2O_5$ | 0.19 | 0.14–0.26 | 0.04 | apatite (*Kα*) | 0.02 | 0.00–0.04 | 0.02 | Y-Phosphate (*Kα*) |
| $Mn_2O_3$ | 7.70 | 7.59–7.82 | 0.11 | rhodonite (*Kα*) | 7.30 | 7.21–7.41 | 0.08 | rhodonite (*Kα*) |
| $Al_2O_3$ | 0.50 | 0.47–0.54 | 0.03 | $Al_2O_3$ (*Kα*) | 3.40 | 3.27–3.52 | 0.10 | Al–Ca-grossular (*Kα*) |
| $Fe_2O_3$** | 1.63 | 1.58–1.72 | 0.06 | $Fe_3O_4$ (*Kα*) | 3.24 | 3.04–3.53 | 0.21 | fayalite (*Kα*) |
| MgO | 0.69 | 0.60–0.77 | 0.07 | MgO (*Kα*) | 0.04 | 0.00–0.10 | 0.04 | olivine (*Kα*) |
| BaO | 47.30 | 46.45–48.36 | 0.82 | baryte (*Lα*) | 1.04 | 0.89–1.07 | 0.13 | sanbornite (*Lα*) |
| SrO | 2.84 | 2.68–3.00 | 0.12 | celestine (*Lα*) | 38.18 | 37.77–38.60 | 0.39 | celestine (*Lα*) |
| CaO | 0.14 | 0.12–0.16 | 0.02 | wollastonite (*Kα*) | 2.25 | 2.10–2.31 | 0.10 | Al–Ca-grossular (*Kα*) |
| PbO | 1.26 | 1.14–1.45 | 0.12 | galena (*Mα*) | 0.38 | 0.14–0.55 | 0.19 | PbO (*Mα*) |
| $Na_2O$ | 0.08 | 0.04–0.13 | 0.04 | jadeite (*Kα*) | | | | |
| $H_2O$* | 1.42 | | | | 1.73 | | | |
| Total | 98.55 | | | | 98.94 | | | |

*Calculated by stoichiometry from the results of the crystal structure analysis; **All Fe and Mn is considered as $Fe^{3+}$ and $Mn^{3+}$ based on experimental and redox potential arguments; S.D. – standard deviation.

Cu and Zn were below the detection limit. Analytical results, standards and spectral line are reported in Table 1. The chemical composition of aldomarinoite was determined by WDS using a Jeol 8200 Super Probe electron microprobe at the University of Milano operating at an acceleration voltage of 15 kV and beam current of 5 nA (beam size = 3 μm). Potassium, Na, Ti, Si and F were below the detection limit of 0.03 atoms per formula unit (apfu). Analytical results, standards and spectral line are reported in Table 1.

Both the analyses were subject to ZAF-corrections using the *PAP* routine (Pouchou and Pichoir, 1985). For both minerals, $H_2O$ was calculated based on one OH group per formula unit (pfu) (see Raman and FTIR spectroscopy sections). Manganese was also considered as $Mn^{3+}$ on the basis of high oxidising environments as well as OAS results. All Fe was considered to be $Fe^{3+}$ based on the Mn and Fe redox potential arguments and site bond length observed from SREF. The empirical formula, calculated on the basis of 9 O apfu, is, within rounding errors, $(Ba_{1.96}Sr_{0.17}Pb_{0.04}Na_{0.02}Ca_{0.02})_{\Sigma 2.21}(Mn^{3+}_{0.62}Fe^{3+}_{0.13}Al_{0.06}Mg_{0.11})_{\Sigma 0.92}[(As_{0.87}V_{0.12}P_{0.01})_{\Sigma 1.00}O_4]_2(OH)$ for lombardoite, and $(Sr_{1.93}Ca_{0.21}Ba_{0.04}Pb_{0.01})_{\Sigma 2.19}(Mn^{3+}_{0.48}Al_{0.35}Fe^{3+}_{0.21}Mg_{0.01})_{\Sigma 1.05}[(As_{0.92}V_{0.03})_{\Sigma 0.95}O_4]_2(OH)$ for aldomarinoite. The ideal formula for lombardoite is $Ba_2Mn^{3+}(AsO_4)_2(OH)$, which requires BaO 49.11, $Mn_2O_3$ 12.64, $As_2O_5$ 36.81, $H_2O$ 1.44, total 100 wt.%, and for aldomarinoite is $Sr_2Mn^{3+}(AsO_4)_2(OH)$, which requires SrO 40.24, $Mn_2O_3$ 15.32, $As_2O_5$ 42.69, $H_2O$ 1.75, total 100 wt.%. Lombardoite is unreactive and insoluble in 2 M and 10% HCl and 65% $HNO_3$ and aldomarinoite in 37% HCl and 69% $HNO_3$.

## X-ray crystallography

### *Powder X-ray diffraction*

The powder X-ray diffraction pattern of lombardoite was obtained with an Oxford Gemini R Ultra diffractometer equipped with a CCD area detector at CrisDi (University of Turin). Experimental and calculated data are reported in Table 2. The unit-cell parameters refined from the powder data with the software *GSAS* (Larson and Von Dreele, 1994) are: $a = 7.883(2)$ Å, $b = 6.146(1)$ Å, $c = 9.101(2)$ Å, $\beta = 112.52(1)°$ and $V = 407.3(2)$ Å$^3$.

The powder X-ray diffraction data of aldomarinoite were obtained with a Rigaku XtaLAB Synergy-S, equipped with a microfocus Mo*K*α source and a HyPix-6000HE detector with graphite-monochromatised Mo*K*α radiation (University of Milano). Experimental and calculated data are reported in Table 2. The unit-cell parameters refined from the powder data with the software UnitCell (Holland and Redfern, 1997) are: $a = 7.5414(3)$ Å, $b = 5.9838(2)$ Å, $c = 8.7399(3)$ Å, $\beta = 112.034(4)°$ and $V = 365.60(2)$ Å$^3$.

### *Single-crystal X-ray diffraction*

Data for lombardoite were collected using an Oxford Gemini R Ultra diffractometer equipped with a CCD area detector at CrisDi (Università di Torino, Italy), with graphite-monochromatised Mo*K*α radiation. Crystal data and experimental details are reported in Table 3. At room temperature, the unit-cell parameters are: $a = 7.8636(1)$ Å, $b = 6.13418(1)$ Å, $c = 9.1197(1)$ Å, $\beta = 112.660(2)°$, $V = 405.94(1)$ Å$^3$, space group = $P2_1/m$ and $Z = 2$.

Data for aldomarinoite were collected using a Rigaku XtaLAB Synergy-S at the University of Milano, equipped with a microfocus Mo*K*α source and a HyPix-6000HE detector with graphite-monochromatised Mo*K*α radiation. Crystal data and experimental details are reported in Table 3. At room temperature, the unit-cell parameters are: $a = 7.5577(4)$ Å, $b = 5.9978(3)$ Å, $c = 8.7387(4)$ Å, $\beta = 111.938(6)°$, $V = 367.43(3)$ Å$^3$, space group = $P2_1/m$ and $Z = 2$. A total of 1755 independent reflections were collected.

The two structure models were refined starting from the atom coordinates of arsenbrackebuschite (Hofmeister and Tillmanns, 1978) for lombardoite and of grandaite (Cámara *et al.*, 2014) for aldomarinoite, by means of the *SHELX* set of programs (Sheldrick, 2015).

Scattering curves for neutral atoms were taken from the *International Tables for Crystallography* (Wilson, 1992). Site-scattering values were refined for the cation sites using two scattering curves contributing proportionally and by constraining the sum to full occupancy: As and V were used for the *T*(1) and *T*(2) sites; Al and Mn were considered for the *M* site; Ba and Sr were used for the *A*(1) and *A*(2) sites in lombardoite, whereas for aldomarinoite Sr and Ca were used for the *A*(1) site; and Sr and Ba for the *A*(2) site. A peak in the difference-Fourier map was found close to O(7) and added to the model as an H atom with fixed coordinates for aldomarinoite and refined coordinates for lombardoite. An isotropic displacement factor of 1.2 times the one observed for the bonded O(7) anion site, and full occupancy

**Table 2.** Powder X-ray diffraction data ($d$ in Å, $I$ in %) for lombardoite and aldomarinoite*.

| Lombardoite | | | | | | | Aldomarinoite | | | | | | |
|---|---|---|---|---|---|---|---|---|---|---|---|---|---|
| $h$ | $k$ | $l$ | $d_{obs}$ | $d_{calc}$ | $I_{obs}$ | $I_{calc}$ | $h$ | $k$ | $l$ | $d_{obs}$ | $d_{calc}$ | $I_{obs}$ | $I_{calc}$ |
| **1** | **0** | **$\bar{1}$** | **6.985** | **6.986** | **39** | **6.7** | 1 | 0 | $\bar{1}$ | 6.747 | 6.679 | 7 | 1.1 |
| **1** | **1** | **1** | **3.727** | **3.719** | **33** | **14.7** | 0 | 1 | 1 | 4.835 | 4.821 | 13 | 3.4 |
| **2** | **1** | **$\bar{1}$** | **3.314** | **3.307** | **100** | **100.0** | 1 | 1 | $\bar{1}$ | 4.472 | 4.463 | 13 | 2.4 |
| **0** | **2** | **0** | **3.073** | **3.067** | **24** | **37.6** | 1 | 1 | 1 | 3.615 | 3.615 | 10 | 9.9 |
| **2** | **1** | **$\bar{2}$** | **3.036** | **3.035** | **33** | **53.0** | 2 | 0 | 0 | 3.486 | 3.505 | 7 | 7.1 |
| **1** | **0** | **$\bar{3}$** | **3.034** | **3.040** | | | **2** | **1** | **$\bar{1}$** | **3.191** | **3.193** | **89** | **100.0** |
| 2 | 0 | 1 | 2.954 | 2.945 | 6 | 5.4 | **0** | **2** | **0** | **2.997** | **2.999** | **45** | **39.3** |
| 0 | 2 | 1 | 2.886 | 2.882 | 10 | 9.7 | **2** | **1** | **$\bar{2}$** | **2.914** | **2.918** | **47** | **42.4** |
| 1 | 2 | 0 | 2.831 | 2.825 | 6 | 5.0 | 1 | 0 | $\bar{3}$ | | 2.913 | | |
| **1** | **2** | **$\bar{1}$** | **2.813** | **2.808** | **87** | **67.8** | 0 | 2 | 1 | 2.806 | 2.813 | 13 | 8.5 |
| **1** | **1** | **2** | **2.807** | **2.803** | | | **1** | **1** | **2** | **2.715** | **2.718** | **100** | **64.5** |
| 2 | 1 | 1 | 2.662 | 2.655 | 19 | 9.7 | 2 | 1 | 1 | 2.569 | 2.576 | 11 | 11.6 |
| 2 | 1 | $\bar{3}$ | 2.547 | 2.549 | 6 | 8.6 | 1 | 2 | 1 | 2.492 | 2.501 | 15 | 9.6 |
| 3 | 0 | 0 | 2.427 | 2.419 | 6 | 5.1 | 2 | 1 | $\bar{3}$ | 2.444 | 2.445 | 24 | 10.6 |
| 2 | 2 | 0 | 2.348 | 2.342 | 13 | 11.7 | 3 | 0 | 0 | 2.328 | 2.337 | 8 | 4.1 |
| 1 | 2 | $\bar{3}$ | 2.159 | 2.159 | 19 | 27.5 | **1** | **2** | **$\bar{3}$** | **2.087** | **2.089** | **39** | **27.6** |
| 3 | 0 | 1 | 2.125 | 2.118 | 20 | 12.4 | 2 | 2 | $\bar{3}$ | 1.994 | 1.997 | 6 | 3.0 |
| 1 | 1 | $\bar{4}$ | 2.124 | 2.127 | | | 4 | 0 | $\bar{2}$ | 1.882 | 1.886 | 17 | 10.5 |
| 4 | 0 | $\bar{2}$ | 1.968 | 1.964 | 18 | 9.9 | **3** | 1 | $\bar{4}$ | **1.833** | **1.836** | **32** | **17.2** |
| 3 | 1 | $\bar{4}$ | 1.916 | 1.918 | 18 | 17.3 | 2 | 3 | $\bar{1}$ | 1.761 | 1.766 | 29 | 12.2 |
| 2 | 3 | $\bar{1}$ | 1.817 | 1.814 | 17 | 13.4 | **3** | **2** | **1** | **1.689** | **1.693** | **36** | **20.0** |
| 1 | 1 | 4 | 1.763 | 1.763 | 7 | 4.7 | **1** | **3** | **2** | **1.664** | **1.672** | **21** | **13.2** |
| **3** | **2** | **1** | **1.748** | **1.743** | **24** | **17.3** | 4 | 2 | $\bar{2}$ | 1.595 | 1.596 | 27 | 10.1 |
| 1 | 3 | 2 | 1.718 | 1.715 | 19 | 13.3 | 0 | 1 | 5 | 1.560 | 1.565 | 6 | 4.2 |
| 4 | 2 | $\bar{2}$ | 1.657 | 1.654 | 11 | 11.1 | 0 | 4 | 0 | 1.498 | 1.499 | 28 | 9.2 |
| 1 | 2 | $\bar{5}$ | 1.551 | 1.552 | 6 | 5.6 | 2 | 0 | $\bar{6}$ | 1.454 | 1.456 | 8 | 3.8 |
| 0 | 4 | 0 | 1.537 | 1.534 | 9 | 8.7 | 3 | 3 | $\bar{4}$ | 1.385 | 1.388 | 21 | 6.2 |
| 3 | 3 | $\bar{4}$ | 1.437 | 1.437 | 8 | 6.7 | 5 | 1 | 0 | 1.359 | 1.365 | 11 | 4.9 |
| 5 | 1 | 0 | 1.417 | 1.412 | 8 | 5.2 | 2 | 2 | 4 | 1.360 | 1.359 | 8 | 6.7 |
| 2 | 2 | 4 | 1.403 | 1.402 | 11 | 6.9 | 1 | 4 | $\bar{3}$ | 1.329 | 1.333 | 18 | 5.5 |
| 1 | 4 | $\bar{3}$ | 1.371 | 1.369 | 7 | 6.3 | 2 | 2 | $\bar{6}$ | 1.310 | 1.310 | 8 | 3.0 |
| 6 | 1 | $\bar{3}$ | 1.283 | 1.280 | 8 | 4.7 | 3 | 3 | $\bar{5}$ | 1.278 | 1.274 | 5 | 0.8 |
| 5 | 2 | $\bar{5}$ | 1.272 | 1.272 | 7 | 5.6 | 0 | 3 | 5 | 1.259 | 1.259 | 7 | 2.0 |
| | | | | | | | 5 | 2 | $\bar{5}$ | 1.221 | 1.220 | 21 | 4.9 |
| | | | | | | | 4 | 4 | $\bar{2}$ | 1.171 | 1.174 | 19 | 2.8 |
| | | | | | | | 0 | 1 | 7 | 1.137 | 1.137 | 10 | 2.7 |

*Only reflections with $I_{rel}$ > 5%($I_{rel}$) are listed; the strongest reflections are in bold.

were applied. Refinement converged to $R_1 = 0.0197$ for 2628 observed reflections with $F_o > 4\sigma(F_o)$ and 87 parameters for lombardoite and to $R_1 = 0.0345$ for 1235 observed reflections with $F_o > 4\sigma(F_o)$ and 83 parameters for aldomarinoite. Tables 4, 5 and 6 report, respectively, atom coordinates, displacement parameters, and selected bond distances and angles. Bond valence calculations using the parameters of Gagné and Hawthorne (2015) are reported in Table 4. The crystallographic information file has been deposited with the Principal Editor of *Mineralogical Magazine* and is available as Supplementary material (see below).

## Description of the structure

### Cation sites

#### M sites

There is one $M$ site hosting small high-charge cations in octahedral coordination. The observed site scattering value 22.576(3) eps (electrons per site) at the $M$ site of lombardoite and 20.49(7) eps at the $M$ site of aldomarinoite agree with the chemical data confirming a Mn dominance at that site. Those correspond to $(Mn^{3+}_{0.67} + Fe^{3+}_{0.14} + Mg_{0.12} + Al_{0.07})_{\Sigma 1.00}$ apfu and 22.50 eps, and $(Mn^{3+}_{0.46} + Al_{0.33} + Fe^{3+}_{0.20} + Mg_{0.01})_{\Sigma 1.00}$ apfu and 21.11 eps, respectively.

The observed average bond length at $M$ sites (2.030 Å for lombardoite and 1.981 Å for aldomarinoite, Table 6) is too small for the $Fe^{2+}$ and $Mn^{2+}$ ions; the incident bond valence sum at the $M$ site is in agreement with average formal charge being dominantly +3, i.e. considering both $Fe^{3+}$ and $Mn^{3+}$ at the $M$ sites, which also agrees with the oxidised nature of the ore.

#### A sites

There are two non-equivalent sites hosting large divalent cations in eight and eleven coordination: the $A(1)$ and $A(2)$ sites, respectively. Site distribution at the $A$ sites was obtained according to the SREF results that show little difference in scattering values at both sites of lombardoite: 53.44(1) eps at the $A(1)$ site, and 54.93(2) eps at the $A(2)$. Therefore, we assign $(Ba_{0.94}Sr_{0.06})$ to $A(1)$ and $(Ba_{1.00})$ to $A(2)$. Also the $A$ site occupancies of aldomarinoite show little difference in the scattering values: 35.05(9) eps at the $A(1)$ site and 38.70(7) eps at the $A(2)$ site. Therefore, we assign $(Sr_{0.81}Ca_{0.19})$ to $A(1)$ and $(Sr_{0.96}Ba_{0.04})$ to $A(2)$. Bond valence calculations indicate that both the $A(1)$ and $A(2)$ sites are compatible with the dominance of divalent cations at these sites.

#### T sites

There are two non-equivalent sites hosting a high charge cation in tetrahedral coordination: the $T(1)$ and the $T(2)$ sites. The refined

**Table 3.** Crystal data and summary of parameters describing data collection and refinement for lombardoite and aldomarinoite.

| | Lombardoite | Aldomarinoite |
|---|---|---|
| **Crystal data** | | |
| Crystal system | Monoclinic | Monoclinic |
| Space group | $P2_1/m$ | $P2_1/m$ |
| Unit-cell dimensions | | |
| $a$ (Å) | 7.8636(1) | 7.5577(4) |
| $b$ (Å) | 6.13421(8) | 5.9978(3) |
| $c$ (Å) | 9.1197(1) | 8.7387(4) |
| β (°) | 112.660(2) | 111.938(6) |
| $V$ (Å$^3$) | 405.94(1) | 367.43(3) |
| $Z$ | 2 | 2 |
| μ (mm$^{-1}$) | 18.21 | 23.31 |
| $F$(000) | 532 | 466 |
| $D_{calc}$ (g cm$^{-3}$) | 5.124 | 4.679 |
| **Data collection** | | |
| Crystal size (mm) | 0.078 × 0.096 × 0.156 | 0.097 × 0.102 × 0.128 |
| Radiation type (λ) | Mo$K\alpha$ (0.71073 Å) | Mo$K\alpha$ (0.71073 Å) |
| Temperature (K) | 298 | 298 |
| θ range for data collection (°) | 4.1–40.9 | 2.5–35.0 |
| $R_{int}$ | 0.0368 | 0.0614 |
| Reflections collected | 2808 | 1755 |
| Independent reflections $F_o$>4σ($F$) | 2628 | 1235 |
| **Refinement** | | |
| Refinement method | least-squares matrix: full | least-squares matrix: full |
| No. of refined parameters | 87 | 83 |
| Final $R_{obs}$ | 0.0228 | 0.0622 |
| $R_1$ | 0.0197 | 0.0345 |
| $wR_2$ $F_o$>4σ($F$) | 0.0449 | 0.0792 |
| Highest peak/deepest hole ($e^-$ Å$^{-3}$) | +1.14 / −1.11 | +1.37 / −1.23 |
| Goodness of fit on $F^2$ | 1.155 | 1.101 |

site scattering values obtained for $T$ sites are 31.26(3) for $T$(1) and 31.11(4) for $T$(2) of lombardoite, and 32.9 for $T$(1) and 32.8 for $T$(2) of aldomarinoite, are quite similar, whereas average bond lengths and distortion parameters are significantly different (Table 6). The limited quantity of V observed in the chemical analyses (Table 1) and the absence of high-charge cations ($Si^{4+}$, $P^{5+}$, $S^{6+}$) that may potentially occupy the $T$ sites suggests V disordered equally at the $T$(1,2) sites. The distortion is therefore ascribed to the different $A$-polyhedron size due to the $Ba_{-1}Sr$ substitution: the smaller $A(1)O_8$ and $A(2)O_{11}$ polyhedra in aldomarinoite yield a larger distortion of As-centred tetrahedra, in particular of $T$(1)O4 tetrahedron because of the O(5) atom acting as donor of charge for the hydrogen bond (see below).

The cation part of the structure is represented by $[Mn^{3+}(Ba^{2+}, Sr^{2+})_2As_2^{5+}]^{\Sigma 17+}$.

### *Anion sites*

There are seven anion positions in the structure of lombardoite and aldomarinoite, two of them on general position, accounting for a total of 18 anions per unit cell. Bond valence data (Table 4) show that one out of seven anions sites has bond valence sum close to 2 vu (valence units), whereas the O(7) site has a smaller contribution (1.341 vu for lombardoite and 1.400 vu for aldomarinoite) compatible with the occurrence of monovalent anion at this site. The absence of F in the chemical analyses (Table 1) indicates that the O(7) site must therefore host a hydroxyl group. In fact, a maxima was found in the Fourier difference and added to the model as atom H(7). The hydrogen at H(7) is at 1.64 Å from the O(5) atom, which has a bond-valence sum of 1.503 vu for lombardoite and is at 1.791 Å from the O(5)

**Table 4.** Wyckoff numbers, fractional atom coordinates, and equivalent isotropic displacement parameters (Å$^2$) for lombardoite and aldomarinoite*. Bond valence sums (BVS, in valence units) calculated using the parameters of Gagné and Hawthorne (2015).

| Site | Wyckoff no. | BVS | Occupancy | $x/a$ | $y/b$ | $z/c$ | $U_{iso}$ |
|---|---|---|---|---|---|---|---|
| **Lombardoite** | | | | | | | |
| $T$(1) | 2*e* | 4.974 | 0.826(8)As, 0.174(8)V | 0.44056(3) | ¼ | 0.17071(3) | 0.00958(6) |
| $T$(2) | 2*e* | 4.976 | 0.811(7)As, 0.189(7)V | 0.04478(3) | ¼ | 0.33315(3) | 0.00793(6) |
| $M$ | 2*a* | 2.735 | 0.202(7)Al, 0.798(7)Mn | 0 | 0 | 0 | 0.00893(9) |
| $A$(1) | 2*e* | 1.994 | 0.858(8)Ba, 0.142(8)Sr | 0.26280(2) | ¼ | 0.750836(18) | 0.01778(5) |
| $A$(2) | 2*e* | 2.188 | 0.931(8)Ba, 0.069(8)Sr | 0.677229(19) | ¼ | 0.586208(15) | 0.01073(4) |
| O(1) | 4*f* | 2.087 | | −0.00460(19) | 0.5196(2) | 0.78247(15) | 0.0150(2) |
| O(2) | 2*e* | 1.873 | | 0.2665(3) | ¼ | 0.4554(2) | 0.0193(4) |
| O(3) | 2*e* | 1.874 | | 0.9107(3) | ¼ | 0.4355(3) | 0.0263(5) |
| O(4) | 4*f* | 2.121 | | 0.49569(19) | 0.0284(2) | 0.28672(16) | 0.0163(2) |
| O(5) | 2*e* | 1.504 | | 0.5530(3) | ¼ | 0.0463(3) | 0.0398(8) |
| O(6) | 2*e* | 1.756 | | 0.2098(2) | ¼ | 0.0488(2) | 0.0141(3) |
| O(7) | 2*e* | 1.339 | | 0.8356(2) | ¼ | 0.9331(2) | 0.0113(3) |
| H(7) | 2*e* | 0.866 | 1 | 0.733(5) | ¼ | 0.996(5) | 0.014 |
| **Aldomarinoite** | | | | | | | |
| $T$(1) | 2*e* | 5.085 | 0.99As, 0.01V | 0.44423(7) | ¼ | 0.17242(6) | 0.01399(14) |
| $T$(2) | 2*e* | 5.148 | 0.98As, 0.02V | 0.03634(7) | ¼ | 0.33908(6) | 0.01223(13) |
| $M$ | 2*a* | 3.022 | 0.624(6)Mn, 0.376(6)Al | 0 | 0 | 0 | 0.0133(4) |
| $A$(1) | 2*e* | 1.860 | 0.836(5)Sr, 0.164(5)Ca | 0.26613(7) | ¼ | 0.74843(6) | 0.0210(2) |
| $A$(2) | 2*e* | 2.115 | 0.961(4)Sr, 0.039(4)Ba | 0.67213(7) | ¼ | 0.58721(6) | 0.0161(2) |
| O(1) | 4*f* | 2.093 | | 0.0129(4) | 0.5161(4) | 0.7816(3) | 0.0189(5) |
| O(2) | 2*e* | 1.927 | | 0.2648(5) | ¼ | 0.4566(5) | 0.0276(8) |
| O(3) | 2*e* | 1.887 | | 0.9087(6) | ¼ | 0.4556(5) | 0.0281(9) |
| O(4) | 4*f* | 2.070 | | 0.5033(3) | 0.0241(4) | 0.2932(3) | 0.0191(5) |
| O(5) | 2*e* | 1.876 | | 0.5436(6) | ¼ | 0.0326(5) | 0.0313(10) |
| O(6) | 2*e* | 1.972 | | 0.2033(5) | ¼ | 0.0551(4) | 0.0210(8) |
| O(7) | 2*e* | 1.400 | | 0.8305(4) | ¼ | 0.9233(4) | 0.0120(6) |
| H(7) | 2*e* | 0.533 | 1 | 0.7324 | ¼ | 0.9555 | 0.014 |

*The temperature factor has the form exp(−$T$) where $T = 8\pi^2U(\sin(\theta)/\lambda)^2$ for isotropic atoms.

**Table 5.** Anisotropic displacement parameters (Å$^2$) for lombardoite and aldomarinoite*.

| Site | $U^{11}$ | $U^{22}$ | $U^{33}$ | $U^{23}$ | $U^{13}$ | $U^{12}$ |
|---|---|---|---|---|---|---|
| **Lombardoite** | | | | | | |
| *T*(1) | 0.00983(11) | 0.01016(10) | 0.00751(9) | 0 | 0.00196(7) | 0 |
| *T*(2) | 0.00947(11) | 0.00762(9) | 0.00715(9) | 0 | 0.00369(7) | 0 |
| *M* | 0.01248(17) | 0.00694(13) | 0.00692(14) | 0.00018(9) | 0.00325(11) | 0.00034(10) |
| *A*(1) | 0.01704(8) | 0.02484(8) | 0.01610(7) | 0 | 0.01152(6) | 0 |
| *A*(2) | 0.01133(6) | 0.01183(5) | 0.00941(5) | 0 | 0.00440(4) | 0 |
| O(1) | 0.0230(6) | 0.0101(4) | 0.0123(4) | 0.0011(4) | 0.0071(4) | 0.0014(4) |
| O(2) | 0.0131(7) | 0.0266(9) | 0.0154(7) | 0 | 0.0025(6) | 0 |
| O(3) | 0.0267(10) | 0.0361(12) | 0.0251(10) | 0 | 0.0200(9) | 0 |
| O(4) | 0.0171(5) | 0.0125(5) | 0.0159(5) | 0.0029(4) | 0.0026(4) | 0.0020(4) |
| O(5) | 0.0217(11) | 0.085(2) | 0.0194(9) | 0 | 0.0146(8) | 0 |
| O(6) | 0.0114(7) | 0.0151(7) | 0.0131(6) | 0 | 0.0018(5) | 0 |
| O(7) | 0.0104(6) | 0.0116(6) | 0.0115(6) | 0 | 0.0038(5) | 0 |
| **Aldomarinoite** | | | | | | |
| *T*(1) | 0.0137(3) | 0.0155(2) | 0.0114(2) | 0 | 0.00304(19) | 0 |
| *T*(2) | 0.0134(3) | 0.0133(2) | 0.0103(2) | 0 | 0.00476(19) | 0 |
| *M* | 0.0137(4) | 0.0116(4) | 0.0088(4) | 0.0001(3) | 0.0031(3) | −0.0002(3) |
| *A*(1) | 0.0176(3) | 0.0263(3) | 0.0199(3) | 0 | 0.0109(2) | 0 |
| *A*(2) | 0.0163(2) | 0.0193(3) | 0.0139(2) | 0 | 0.00707(18) | 0 |
| O(1) | 0.0310(15) | 0.0129(11) | 0.0137(11) | 0.0013(9) | 0.0096(11) | 0.0000(10) |
| O(2) | 0.0120(18) | 0.041(2) | 0.023(2) | 0 | −0.0013(15) | 0 |
| O(3) | 0.032(2) | 0.034(2) | 0.029(2) | 0 | 0.0235(19) | 0 |
| O(4) | 0.0223(13) | 0.0168(12) | 0.0160(11) | 0.0027(10) | 0.0046(10) | 0.0006(10) |
| O(5) | 0.030(2) | 0.051(2) | 0.023(2) | 0 | 0.0209(19) | 0 |
| O(6) | 0.0182(18) | 0.0257(18) | 0.0148(18) | 0 | 0.0013(14) | 0 |
| O(7) | 0.0094(15) | 0.0108(15) | 0.0165(16) | 0 | 0.0058(13) | 0 |

*The temperature factor has the form exp(−*T*) where $T = 2\pi^2\Sigma_{ij}(h_{(i)}h_{(j)}U_{(i,j)}a^*_{(i)}a^*_{(j)})$.

**Table 6.** Selected interatomic distances (Å) and angles (°) for lombardoite and aldomarinoite*.

| | Lombardoite | Aldomarinoite | | Lombardoite | Aldomarinoite |
|---|---|---|---|---|---|
| *T*(1)−O(4) (×2) | 1.674(1) | 1.673(2) | *A*(1)−O(4)(×2) | 2.673(1) | 2.519(2) |
| *T*(1)−O(5) | 1.686(2) | 1.656(3) | *A*(1)−O(5) | 2.706(2) | 2.583(4) |
| *T*(1)−O(6) | 1.724(2) | 1.724(3) | *A*(1)−O(1) (×2) | 2.780(3) | 2.590(2) |
| <*T*(1)−O> | 1.690 | 1.681 | *A*(1)−O(2) | 2.776(1) | 2.547(4) |
| *V* (Å$^3$) | 2.47 | 2.43 | *A*(1)−O(3) | 2.903(2) | 2.946(4) |
| $\sigma^{2*}$ | 5.40 | 11.20 | *A*(1)−O(6) | 3.131(3) | 2.891(3) |
| λ * | 1.0015 | 1.0030 | *A*(1)−O> | 2.802 | 2.648 |
| | | | *V* (Å$^3$) | 32.98 | 27.77 |
| *T*(2)−O(3) | 1.655(2) | 1.644(4) | | | |
| *T*(2)−O(2) | 1.669(2) | 1.647(4) | *A*(2)−O(3) | 2.684(2) | 2.460(4) |
| *T*(2)−O(1) (×2) | 1.718(1) | 1.710(2) | *A*(2)−O(4) (×2) | 2.706(1) | 2.566(2) |
| *T*(2)−O> | 1.690 | 1.678 | *A*(2)−O(7) | 2.888(1) | 2.726(3) |
| *V* (Å$^3$) | 2.48 | 2.42 | *A*(2)−O(4) (×2) | 2.919(2) | 2.760(2) |
| $\sigma^{2*}$ | 1.56 | 0.40 | *A*(2)−O(2) | 2.958(1) | 2.855(4) |
| λ * | 1.0008 | 1.0008 | *A*(2)−O(1) (×2) | 2.981(2) | 2.966(2) |
| | | | *A*(2)−O2 (×2) | 3.1427(5) | 3.083(2) |
| *M*−O(7) (×2) | 1.946(1) | 1.923(2) | <*A*(2)−O> | 2.907 | 2.799 |
| *M*−O(1) (×2) | 1.974(1) | 1.949(2) | *V* (Å$^3$) | 54.80 | 48.52 |
| *M*−O(6) (×2) | 2.169(1) | 2.071(3) | | | |
| <*M*−O> | 2.030 | 1.981 | O(7)−H(7) | 1.16(4) | 0.886(3) |
| *V* (Å$^3$) | 11.01 | 10.23 | O(7)···O(5) | 2.788(3) | 2.676(7) |
| $\sigma^{2*}$ | 22.64 | 28.06 | O(5)···H(7) | 1.64(4) | 1.791(6) |
| λ * | 1.0111 | 1.0099 | O(7)−H−O(5) | 168(3)° | 176.7(3)° |

*Mean quadratic elongation (λ) and the angle variance ($\sigma^2$, in °^2) were computed according to Robinson *et al.* (1971).

atom, which has a bond-valence sum of 1.619 vu for aldomarinoite, and so is likely to receive a hydrogen bond. Therefore there is a hydrogen bond with oxygen at O(5) ensuring a further contribution of bond valence to this site (Table 7). The structural model, thus, confirms O–H···O = 2.8 Å for lombardoite, in good agreement with IR data, and O–H···O = 2.7 Å for aldomarinoite. The anion part of the structure is represented by $[O_8(OH)]^{\Sigma17-}$.

### *Structure topology*

The crystal structures of lombardoite and aldomarinoite (Fig. 8) are topologically identical to that of arsenbrackebuschite. Chains of $[M^{3+(2+)}(T^{5+}O_4)_2(OH,H_2O)]$ units are connected through interstitial divalent cations. The $M^{3+}O_6$ octahedron shares edges with other octahedra forming a chain along [010]. The shared

**Table 7.** The brackebuschite supergroup, $A(1)^{2+}A(2)^{2+}[^{VI}M_x^{3+}\ ^{VI}M_{1-x}^{2+}][^{IV}(T_x^{5+}T_{1-x}^{6+})O_4]_2X$ (references are given in brackets).

| Arsenbrackebuschite group dominant at $T$ = As | Brackebuschite group dominant at $T$ = V | Goedkenite group dominant at $T$ = P | Tsumebite group dominant at $T$ = (P or As) + (S or V) |
|---|---|---|---|
| Arsenbrackebuschite [1][2] | Brackebuschite [6][8][9][10][11][31] | Bearthite [18][19][20] | Arsentsumebite [3][4][5] |
| $Pb_2Fe^{3+}(AsO_4)_2(OH,H_2O)$ | $Pb_2Mn^{3+}(VO_4)_2(OH)$ | $Ca_2Al(PO_4)_2(OH)$ | $Pb_2Cu[(AsO_4)(SO_4)](OH)$ |
| Feinglosite [7] | Calderónite* [12] | Goedkenite [24] | Bushmakinite [21][22][23] |
| $Pb_2Zn(AsO_4)_2(OH,H_2O)$ | $Pb_2Fe^{3+}(VO_4)_2(OH)$ | $Sr_2Al(PO_4)_2(OH)$ | $Pb_2Al[(PO_4)(VO_4)](OH)$ |
| Grandaite [29] | Gamagarite [13][14][15] | | Ferribushmakinite [30] |
| $Sr_2Al(AsO_4)_2(OH)$ | $Ba_2Fe^{3+}(VO_4)_2(OH,H_2O)$ | | $Pb_2Fe^{3+}[(PO_4)(VO_4)](OH)$ |
| Canosioite [32] | Heyite* [16][30] | | Tsumebite [10][25][25][25][28] |
| $Ba_2Fe^{3+}(AsO_4)_2(OH)$ | $Pb_5Fe_2^{2+}(VO_4)_2O_4$ | | $Pb_2Cu[(PO_4)(SO_4)](OH)$ |
| Lombardoite [33] | Tokyoite [17] | | |
| $Ba_2Mn^{3+}(AsO_4)_2(OH)$ | $Ba_2Mn^{3+}(VO_4)_2(OH)$ | | |
| Aldomarinoite [34] | | | |
| $Sr_2Mn^{3+}(AsO_4)_2(OH)$ | | | |

Refs: [1] Abraham *et al.* (1978); [2] Hofmeister and Tillmanns (1978); [3] Vésignié, J.P.L. (1935); [4] Bideaux *et al.* (1966); [5] Zubkova *et al.* (2002); [6] Brackebusch *et al.* (1883); [7] Clark *et al.* (1997); [8] Rammelsberg (1880); [9] Donaldson and Barnes (1955); [10] Fanfani and Zanazzi (1967); [11] Foley *et al.* (1997); [12] González del Tánago *et al.* (2003); [13] de Villiers (1943); [14] Harlow *et al.* (1984); [15] Basso *et al.* (1987); [16] Williams (1973); [17] Matsubara *et al.* (2004); [18] Brunet *et al.* (1993); [19] Brunet and Chopin (1995); [20] Roth (2007); [21] Pekov *et al.* (2002); [22] Yakubovich *et al.* (2002); [23] Pekov (2007); [24] Moore *et al.* (1975); [25] Rosický (1912); [26] Busz (1912); [26] Spencer (1913); [28] Nichols (1966); [29] Cámara *et al.* (2014); [30] Kampf *et al.* (2015); [31] Lafuente and Downs (2016); [32] Cámara *et al.* (2017); [33] Cámara *et al.* (2016); [34] this study; * recent examination on the holotype specimen (BM1972,194) has confirmed the structural correspondence of heyite and calderónite (Kampf *et al.*, 2015).

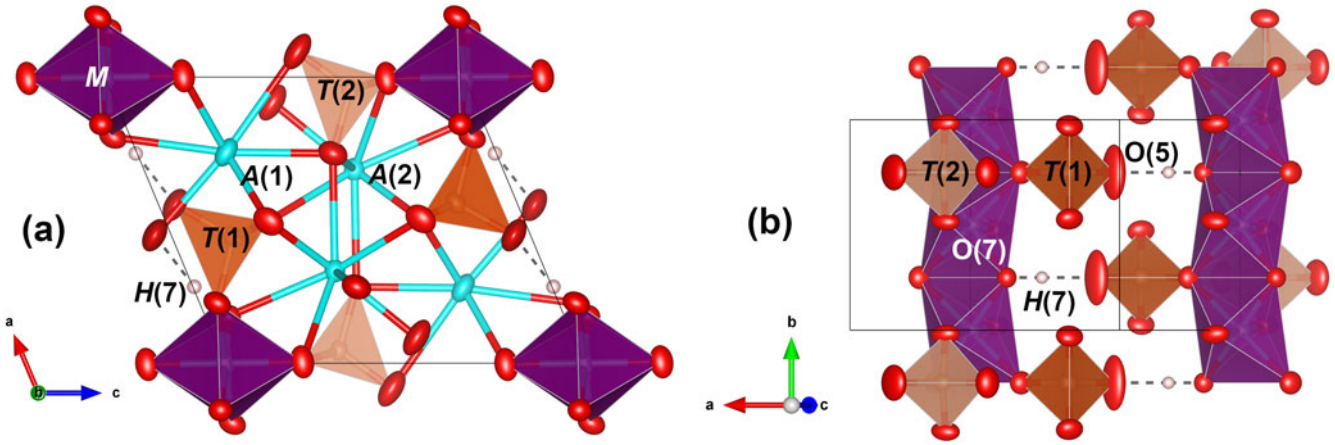


**Fig. 8.** Detail of the lombardoite, and aldomarinoite, structure showing the chains of $Mn^{3+}$ octahedra, $AsO_4$ groups and interstitial large cations, projected onto [010] (a) and [001] (b). Orange: As tetrahedra ($T$(1) and $T$(2)); purple: $Mn^{3+}$ centre $M$ octahedra; cyan: Ba and Sr sites ($A$(1) and $A$(2)); pale pink: H sites; red: oxygen sites. O–H···O bonds are indicated by dotted black lines. Thermal displacement ellipsoids shown at 95% probability.

edge has one anion that can be an (OH) group or a $H_2O$ group, depending on the charge of the $M$-cation at the octahedron, and the other anion is shared with the apex of a $T^{5+}O_4$ tetrahedron (the $T$(1) site). The remaining 4 anions coordinating the octahedron are linked to the edge of another $T^{5+}O_4$ tetrahedron (the $T$(2) site) alternating in both sides. Minor $V^{5+}$ is disordered among the two arsenate tetrahedra. Decorated chains of octahedra link together through bonding with two symmetrically independent interstitial cations at the $A$(1) and $A$(2) sites, and hydrogen bonding. In arsenbrackebuschite, Pb occupies both the $A$ sites but is shifted off-centre, as usual, for its lone pair configuration. The small quantity of Pb found in lombardoite and aldomarinoite at the $A$(2') site also follows this configuration. The Pb off-centre displacement has been reported previously in the literature [e.g. synthetic $Pb_2(Pb,K)_4[Si_8O_{20}]O$, Moore *et al.*, 1985; Pb replacing Ba in hyalotekite, Moore *et al.*, 1982 and Christy *et al.*, 1998, or Pb replacing REE in lusernaite-(Y), Biagioni *et al.*, 2013]. The distortion observed for the $T(2)O_4$ tetrahedron along with the low bond valence incidence at O(5) represents a stressed environment for the structure of lombardoite and aldomarinoite.

## Related minerals

Lombardoite, $Ba_2Mn^{3+}(AsO_4)_2(OH)$, is the As-dominant analogue of tokyoite, $Ba_2Mn^{3+}(VO_4)_2(OH)$ and the Ba–As-dominant analogue of brackebuschite, $Pb_2Mn^{3+}(VO_4)_2(OH)$. It is the first Mn–As member of the arsenbrackebuschite group in the brackebuschite supergroup (Table 7).

Aldomarinoite, $Sr_2Mn^{3+}(AsO_4)_2(OH)$, is the Sr-dominant analogue of lombardoite, $Ba_2Mn^{3+}(AsO_4)_2(OH)$, and the $Mn^{3+}$-dominant analogue of grandaite, $Sr^2Al^{3+}(AsO_4)_2(OH)$. It is the second Sr member of the arsenbrackebuschite group of the brackebuschite supergroup (Table 7).

In the Strunz System (Strunz and Nickel, 2001) lombardoite and aldomarinoite fit in subdivision 8.B.G, phosphates, *etc.* with additional anions, without $H_2O$, with medium-sized and large cations (OH, *etc.*).

Costin *et al.* (2015) reported an As-rich tokyoite with the formula $(Ba_{1.92}Sr_{0.05}Pb_{0.03})_{\Sigma 2.00}(Mn^{3+}_{0.98}Fe^{3+}_{0.02})_{\Sigma 1.00}[(As_{1.050}V_{0.950})_{\Sigma 2.00}O_8)](OH)$ from a drill core obtained from the Postmasburg area in the Northern Cape Province of South Africa. Their observations indicated a possible replacement of tokyoite by a composition richer

in As, with an almost complete solid solution from a pure tokyoite towards an As-dominant end-member, reaching compositions of almost 50:50. The grains were associated with K-feldspar, serandite, quartz, witherite, tokyoite and noelbensonite. These authors reported cell parameters obtained by electron backscatter diffraction ($a = 9.121$ Å, $b = 6.142$ Å, $c = 7.838$ Å, $\alpha = \gamma = 90°$, $\beta = 112°$, monoclinic and $P2_1/m$ space group), which compare well with the ones we obtained for lombardoite (Table 3). Costin *et al.* (2015) also reported Raman spectra of As-rich tokyoite. The assignment of Raman peaks in As-rich tokyoite was done by similarity with arsentsumebite by Cosin *et al.* (2015), and suggested a possible ordering of the $AsO_4$ and $VO_4$ tetrahedra. In detail, they observed peaks at 308–340 $cm^{-1}$, assigned to $(AsO_4)^{3-}$ bending modes and at 442–460 $cm^{-1}$ assigned to $(AsO_4)^{3-}$ and $(VO_4)^{3-}$ bending modes. Moreover, Cosin *et al.* (2015) also reported four outstanding peaks between 830 $cm^{-1}$ and 935 $cm^{-1}$, a pair between 830–846 $cm^{-1}$ with a weak band at 730 $cm^{-1}$ [symmetrical stretching vibrations and asymmetrical stretching vibrations of $(AsO_4)^{3-}$, respectively], and a pair between 906 and 935 $cm^{-1}$ [symmetrical stretching vibrations and asymmetrical stretching vibrations of $(VO_4)^{3-}$, respectively]. However, the latter two peaks were at higher wave numbers than expected for the $VO_4$ group in brackebuschite, and this was interpreted as due to the Jahn–Teller distortion effects related to $Mn^{3+}$. Though our samples are almost devoid of V, we observe similar peaks, corresponding to symmetric bending modes for $AsO_4$ at 328 $cm^{-1}$ and the most intense band corresponding to symmetric stretching modes for $AsO_4$ at 818 $cm^{-1}$ (with two unresolved shoulders at 871 $cm^{-1}$ and 759 $cm^{-1}$) in lombardoite. The wave numbers for the corresponding band in aldomarinoite are shifted to higher wave numbers (339, 773, 849 and 893 $cm^{-1}$) probably because of the different bond strength with Sr at the *A* sites.

**Acknowledgements.** Referees Igor V. Pekov, Fabrice Dal Bo and Oleg Siidra are thanked for useful suggestions. F.C. and L.B. acknowledges financial support by the grant Ricerca Locale 2020, Università di Milano, and from the Italian Ministry of Education (MUR) through the project "Dipartimenti di Eccellenza 2018–2022". C.B., M.E.C. and G.C.P. acknowledge financial support of AMI – Associazione Micromineralogica Italiana.

**Supplementary material.** To view supplementary material for this article, please visit https://doi.org/10.1180/mgm.2022.31

## References

Abraham K., Kautz K., Tillmanns E. and Walenta K. (1978) Arsenbrackebuschite, $Pb_2(Fe,Zn)(OH,H_2O)[AsO_4]_2$, a new arsenate mineral. *Neues Jahrbuch für Mineralogie, Monatshefte*, 193–196.

Basso R., Palenzona A. and Zefiro L. (1987) Gamagarite: new occurrence and crystal structure refinement. *Neues Jahrbuch für Mineralogie, Monatshefte*, 295–304.

Biagioni C., Bonaccorsi E., Cámara F., Cadoni M., Ciriotti M.E., Bersani D. and Kolitsch U. (2013) Lusernaite-(Y), $Y_4Al(CO_3)_2(OH,F)_{11}\cdot 6H_2O$, a new mineral species from Luserna Valley, Piedmont, Italy: Description and crystal structure. *American Mineralogist*, **98**, 1322–1329.

Bideaux R. A., Nichols M. C. and Williams S. A. (1966) The arsenate analog of tsumebite, a new mineral. *American Mineralogist*, **51**, 258–259.

Brackebusch L., Rammelsberg C., Doering A. and Websky M. (1883) Sobre los vanadatos naturales de las provincias de Córdoba y San Luis (República Argentina). *Boletín de la Academia Nacional de Ciencias* (*Córdoba*), **5**, 439–524 [in Spanish].

Brunet F. and Chopin C. (1995) Bearthite, $Ca_2Al(PO_4)_2OH$: stability, thermodynamic properties and phase relations. *Contributions to Mineralogy and Petrology*, **121**, 258–266.

Brunet F., Gebert W., Medenbach O. and Tillmanns E. (1993) Bearthite, $Ca_2Al[PO_4]_2(OH)$, a new mineral from high-pressure terranes of the western Alps. *Schweizerische Mineralogische und Petrographische Mitteilungen*, **73**, 1–9.

Busz K. (1912) Tsumebit, ein neues Mineral von Otavi und Zinnsteinkristalle. *Deutschen Naturforscher und Ärtze in Münster*, **84**, 230–230 [in German].

Cámara F., Ciriotti M.E., Bittarello E., Nestola F., Bellatreccia F., Massimi F., Radica F., Costa E., Benna P. and Piccoli G.C. (2014) Arsenic-bearing new mineral species from Valletta mine, Maira Valley, Piedmont, Italy: I. Grandaite, $Sr_2Al(AsO_4)_2(OH)$, description and crystal structure. *Mineralogical Magazine*, **78**, 757–774.

Cámara F., Bittarello E., Ciriotti M.E., Nestola F., Radica F. and Marchesini M. (2015) As-bearing new mineral species from Valletta mine, Maira Valley, Piedmont, Italy: II. Braccoite, $NaMn_5^{2+}[Si_5AsO_{17}(OH)](OH)$, description and crystal structure. *Mineralogical Magazine*, **79**, 171–189.

Cámara F., Bosi F., Ciriotti M.E., Bittarello E., Hålenius U. and Balestra C. (2016) Lombardoite IMA 2016–058. CNMNC Newsletter No. 33, October 2016, page 1141. *Mineralogical Magazine*, **80**, 1135–1144.

Cámara F., Bittarello E., Ciriotti M.E., Nestola F., Radica F., Massimi F., Balestra C. and Bracco R. (2017) As-bearing new mineral species from Valletta mine, Maira Valley, Piedmont, Italy: III. Canosioite, $Ba_2Fe^{3+}(AsO_4)_2(OH)$, description and crystal structure. *Mineralogical Magazine*, **81**, 305–317.

Cámara F., Baratelli L., Ciriotti M.E., Nestola F. and Piccoli G.C. (2021) Aldomarinoite, IMA 2021–054. CNMNC Newsletter 63, page 913. *Mineralogical Magazine*, **85**, 910–915.

Christy A.G., Grew E.S., Mayo S.C., Yates M.G. and Belakovskiy D.I. (1998) Hyalotekite, $(Ba,Pb,K)_4(Ca,Y)_2Si_8(B,Be)_2(Si,B)_2O_{28}F$, a tectosilicate related to scapolite: a new structure refinement, phase transitions and a short-range ordered 3*b* superstructure. *Mineralogical Magazine*, **62**, 77–92.

Chukanov N.V., Möhn G., Dal Bo F., Zubkova N.V., Varlamov D.A., Pekov I.V., Jouffret L., Henot J.-M., Chollet P., Vessely Y., Friis H., Ksenofontov D.A., Agakhanov A.A., Britvin S.N., Desor J., Koshlyakova N.N. and Pushcharovsky D.Y. (2021) Oberwolfachite, $SrFe_3^{3+}(AsO_4)(SO_4)(OH)_6$, a new alunite-supergroup mineral from the Clara mine, Schwarzwald, Germany and Monterniers mine, Rhône, France. *Mineralogical Magazine*, **85**, 808–816.

Clark A.M., Criddle A.J., Roberts A.C., Bonardi M. and Moffatt E.A. (1997) Feinglosite, a new mineral related to brackebuschite, from Tsumeb, Namibia. *Mineralogical Magazine*, **61**, 285–289.

Collo E. (1997) *La zona brianzonese del pianoro della Gardetta (Val Maira-CN): analisi geologico stratigrafica e rapporti fra le unità tettoniche*. MSc Thesis, University of Genoa, Italy [in Italian].

Costin G., Fairey B., Tsikos H. and Guscsik A. (2015) Tokyoite, As-rich tokyoite, and noélbensonite: new occurrences from the Postmasburg manganese field, Northern Cape Province, South Africa. *The Canadian Mineralogist*, **53**, 981–990.

Crema G.C., Dal Piaz G.V., Merlo C. and Zanella E. (1971) *Note illustrative della carta geologica d'Italia alla scala 1:100,000. Fogli 78–79–90 Argentera-Dronero-Demonte*. Nuova Tecnica Grafica, Roma.

de Villiers J. E. (1943) Gamagarite, a new vanadium mineral from the Postmasburg manganese deposits. *American Mineralogist*, **28**, 329–335.

Donaldson D.M. and Barnes W.H. (1955) The structures of the minerals of the descloizite group and adelite groups: III – brackenbuschite. *American Mineralogist*, **40**, 597–613.

Fanfani L. and Zanazzi P.F. (1967) Structural similarities of some secondary lead minerals. *Mineralogical Magazine*, **36**, 522–529.

Foley J.A., Hughes J.M. and Lange D. (1997) The atomic arrangement of brackebuschite, redefined as $Pb_2(Mn^{3+},Fe^{3+})(VO_4)_2(OH)$, and comments on $Mn^{3+}$ octahedra. *The Canadian Mineralogist*, **35**, 1027–1033.

Gagné O.C. and Hawthorne F.C. (2015) Comprehensive derivation of bond-valence parameters for ion pairs involving oxygen, *Acta Crystallographica*, **B71**, 562–578.

González del Tánago J., La Iglesia Á., Rius J. and Fernández Santín S. (2003) Calderónite, a new lead-iron-vanadate of the brackebuschite group. *American Mineralogist*, **88**, 1703–1708.

Hak J., Johan Z., Kvaček M. and Liebscher W. (1969) Kemmlitzite, a new mineral of the woodhouseite group. *Neues Jahrbuch für Mineralogie, Monatshefte*, **1969**, 201–212.

Harlow G.E., Dunn P.J. and Rossman G.R. (1984) Gamagarite: a re-examination and comparison with brackebuschite-like minerals. *American Mineralogist*, **69**, 803–806.

Hofmeister W. and Tillmanns E. (1978) Strukturelle untersuchungen an arsen-brackebuschit. *Tschermaks Mineralogische und Petrographische Mitteilungen*, **25**, 153–163 [in German].

Holland T.J.B. and Redfern S.A.T. (1997) Unit cell refinement from powder diffraction data: the use of regression diagnostics. *Mineralogical Magazine*, **61**, 65–77.

Kampf A.R., Adams P.M., Nash B.P. and Marty J. (2015) Ferribushmakinite, $Pb_2Fe^{3+}(PO_4)(VO_4)(OH)$, the $Fe^{3+}$ analogue of bushmakinite from the Silver Coin mine, Valmy, Nevada. *Mineralogical Magazine*, **79**, 661–669.

Kampf A.R., Cámara F., Ciriotti M.E., Nash B.P., Balestra C. and Chiappino L. (2016) Castellaroite, $Mn_3^{2+}(AsO_4)_2{\cdot}4.5H_2O$, a new mineral from Italy related to metaswitzerite. *European Journal of Mineralogy*, **28**, 687–696.

Lafuente B. and Downs R.T. (2016) Redetermination of brackebuschite, $Pb_2Mn^{3+}(VO_4)_2(OH)$. *Acta Crystallographica*, **E72**, 293–296.

Larson A.C. and Von Dreele R.B. (1994) *General Structure Analysis System* (*GSAS*). Los Alamos National Laboratory Report LAUR, 86–748.

Libowitzky E (1999) Correlation of OH stretching frequencies and O–H···O hydrogen bond lengths in minerals. *Monatshefte für Chemie*, **130**, 1047–1059.

Mandarino J.A. (1979) The Gladstone-Dale relationship. Part III. Some general applications. *The Canadian Mineralogist*, **17**, 71–76.

Mandarino J.A. (1981) The Gladstone-Dale relationship. Part IV. The compatibility concept and its application. *The Canadian Mineralogist*, **19**, 441–450.

Matsubara S., Miyawaki R., Yokoyama K., Shimizu M. and Imai H. (2004) Tokyoite, $Ba_2Mn^{3+}(VO_4)_2(OH)$, a new mineral from the Shiromaru mine, Okutama, Tokyo, Japan. *Journal of Mineralogical and Petrological Sciences*, **99**, 363–367.

Mills S.J., Meisser N., Rumsey M.S., Hay D.G., Spratt J., Ansermet S. and Vonlanthen P. (2014) Strontiopharmacosiderite, IMA 2013–101. CNMNC Newsletter No. 19, February 2014, page 166; *Mineralogical Magazine*, **78**, 165–170.

Moore P.B., Irving A.J. and Kampf A.R. (1975) Foggite, $CaAl(OH)_2(H_2O)[PO_4]$; goedkinite, $(Sr,Ca)_2Al(OH)[PO_4]_2$; and samuelsonite $(Ca,Ba)Fe_2^{2+}Mn_2^{2+}Ca_8Al_2(OH)_2[PO_4]_{10}$: Three new species from the Palermo No. 1 Pegmatite, North Groton, New Hampshire. *American Mineralogist*, **60**, 957–964.

Moore P.B., Araki T. and Ghose S. (1982) Hyalotekite, a complex lead borosilicate: its crystal structure and the lone-pair effect of Pb(II). *American Mineralogist*, **67**, 1012–1020.

Moore P.B., Sen Gupta P.K. and Schlemper E.O. (1985) Solid solution in plumbous potassium oxysilicate affected by interaction of a lone pair with bond pairs. *Nature*, **318**, 548.

Nichols M.C. (1966) The structure of tsumebite. *American Mineralogist*, **51**, 267–267.

Pekov I.V. (2007) New minerals from former Soviet Union countries, 1998–2006: new minerals approved by the IMA Commission on New Minerals and Mineral Names. *Mineralogical Almanac*, **11**, 9–51.

Pekov I.V., Kleimenov D.A., Chukanov N.V., Yakubovich O.V., Massa W., Belakovskiy D.I. and Pautov L.A. (2002) Bushmakinite $Pb_2Al(PO_4)(VO_4)(OH)$, a new mineral of the brackebuschite group from oxidized zone of Berezovskoye gold deposit, the Middle Urals. *Zapiski Vserossijskogo Mineralogicheskogo Obshchestva*, **131**, 62–71.

Pouchou J.L. and Pichoir F. (1985) 'PAP' $\Phi(\rho Z)$ procedure for improved quantitative microanalysis. In J.T. Armstrong, Ed., *Microbeam Analysis*, p. 104–106. San Francisco Press.

Rammelsberg C. (1880) Ueber die vanadinerze aus dem Staat Córdoba in Argentinien. *Zeitschrift der Deutschen Geologischen Gesellschaft*, **32**, 708–713 [in German].

Robinson K., Gibbs G.V. and Ribbe P.H. (1971) Quadratic elongation: a quantitative measure of distortion in coordination polyhedra. *Science*, **172**, 567–570.

Rosický V. (1912) Preslit, ein neues Mineral von Tsumeb in Deutsch-Südwestafrika. *Zeitschrift für Krystallographie und Mineralogie*, **51**, 521–526 [in German].

Roth P. (2007) Bearthite. Pp. 44–45 in: *Minerals First Discovered in Switzerland and Minerals Named after Swiss Individuals*. Kristallografik Verlag, Achberg, Germany, 239 pp.

Roth P., Meisser N., Nestola F., Škoda R., Cámara F., Bosi F., Ciriotti M.E., Hålenius U., Schnyder C. and Bracco R. (2020) Rüdlingerite, $Mn_2^{2+}V^{5+}As^{5+}O_7{\cdot}2H_2O$, a new species isostructural with fianelite. *Minerals*, **10**, 960.

Sheldrick G.M. (2015) Crystal structure refinement with SHELX. *Acta Crystallographica*, **C71**, 3–8.

Smith G., Hålenius U. and Langer K. (1982) Low-temperature spectral studies of $Mn^{3+}$-bearing andalusite- and epidote-type minerals in the range 30,000–5,000 $cm^{-1}$. *Physics and Chemistry of Minerals*, **8**, 136–142.

Spencer L.J. (1913) A (sixth) list of new mineral names. *Mineralogical Magazine*, **16**, 352–378.

Steven C.J. and Gunter M.E. (2018) EXCELIBR: An Excel Spreadsheet for Solving the Optical Orientation of Uniaxial and Biaxial Crystals, *The Microscope*, **65**(4), 147–152.

Strunz H. and Nickel E.H. (2001) *Strunz Mineralogical Tables. Chemical Structural Mineral Classification System*. *9th Edition*. E. Schweizerbart, Stuttgart, Germany, 870 pp.

Vésignié J.P.L. (1935) Présentation d'échantillons. *Bulletin de la Société Française de Minéralogie*, **58**, 4–5 [in French].

Walenta K. and Dunn P.J. (1984) Arsenogoyazit, ein neues mineral der Crandallitgruppe aus dem Schwarzwald. *Schweizerische Mineralogische und Petrographische Mitteilungen*, **64**, 11–19.

Williams S.A. (1973) Heyite, $Pb_5Fe_2(VO_4)_2O_4$, a new mineral from Nevada. *Mineralogical Magazine*, **39**, 65–68.

Wilson A.J.C. (1992) *International Tables for Crystallography, Volume C: Mathematical, physical and chemical tables*. Kluwer Academic, Dordrecht, the Netherlands, 883 pp.

Yakubovich O.V., Massa W. and Pekov I.V. (2002) Crystal structure of the new mineral bushmakinite, $Pb_2\{(Al,Cu)[PO_4][(V,Cr,P)O_4](OH)\}$. *Doklady Earth Sciences*, **382**, 100–105 [in Russian].

Zubkova N.V., Pushcharovsky D.Y., Giester G., Tillmanns E., Pekov I.V. and Kleimenov D.A. (2002) The crystal structure of arsentsumebite, $Pb_2Cu[(As,S)O_4]_2(OH)$. *Mineralogy and Petrology*, **75**, 79–88.